Utrecht University

Institute for Theoretical Physics (ITP)

Theoretical Physics master thesis

Hydrodynamic behaviour and phase transitions of a non-conformal plasma

By:

Guillem Pérez Martín

Student number: 8976848

Supervisors:

Wilke van der Schee, Javier Subils, Umut Gursoy

July 12, 2024

Abstract

The AdS-CFT correspondence has provided new opportunities to study dynamics in strongly coupled theories. In particular, boost-invariant solutions allow us to model heavy-ion collisions.

In this project I will give an overview of the duality, construct an holographic model and study its thermodynamical structure and phase transitions. Then, I will consider a boost-invariant plasma and study if its microscopic evolution, given holographically, is well described by hydrodynamics. Finally I ask whether phase transitions can be probed in this context.

Contents

1 Introduction

One of the main hot topics in high energy physics is understanding heavy ion collisions, and the expanding quark gluon plasma (QGP) resulting from them. Specifically there is interest in understanding if this plasma can be well described by hydrodynamics, and the phase transitions that occur during its cooling stages such as hadronization. One of the main problems with doing this is that quantum chromodynamics (QCD) is a strongly coupled QFT, and unlike in weakly coupled QFTs we cannot take a perturbative approach and usual techniques such as Feynman diagrams no longer apply. Therefore we must use new techniques such as lattice QCD or holography, and in this project we will be interested in the latter.

Holography was first proposed by Maldacena in 19998 [15] and it states that there is a duality between a CFT living in d dimensions and a gravitational theory living in a $d+1$ Anti-de Sitter spacetime. The CFT will reside in the boundary of the AdS_{d+1}, and we will call the AdS_{d+1} spacetime governed by gravity the bulk. It can be used for many different settings, but we are interested in the case where it relates a strongly coupled CFT such as QCD to a weakly coupled theory of gravity. This is really useful because although we cannot directly study the CFT itself we can compute the properties and evolution of the weakly coupled AdS space time through Einstein's equations. Then by studying how the space time behaves at the boundary we can obtain the evolution of the strongly coupled theory.

This duality has been used to study many different CFTs, specially $\mathcal{N} = 4$ super Yang Mills theory (SYM), but we are interested in non conformal theories to study the behaviour of hot QGP. This theory is almost conformal at really high energies, and although some collisions can reach this conformal energy scale, as they cool they explore the non conformal region of the theory and it must be studied. Indeed, as seen in [16] the bulk viscosity plays an important role in the hydrodynamic description of the cooling of QGP, which can only happen in non-conformal theories.

In this project we will study a simple holographic model with a scalar field to break conformality, characterized by a source Λ. We will then compute its equilibrium solutions to study the thermodynamic properties and the transport coefficients of this model as a

function the parameters of the scalar field potential. We will also see how for a certain range of these parameters the system undergoes a second and a first order phase transition. Then we will study the hydrodynamics of a boost invariant plasma and compute the hydrodynamic pressures as a function of energy. Finally we will implement a numerical simulation to dynamically evolve our system, and study if it can be described by our hydrodynamic model as it cools down and how it behaves around the phase transition.

2 Model

To explore the behaviour of this system we will develop a model for the bulk theory. Let us start by writing the action for a scalar field coupled to gravity in five dimensions, which will break conformality.

$$S = \frac{2}{\kappa_5^2}\int d^5x\sqrt{-G}\left[\frac{1}{4}\mathcal{R} - \frac{1}{2}(\nabla\phi)^2 - V(\phi)\right] \tag{2.1}$$

Where the potential is given in terms of a superpotential characterized by two parameters λ_4 and λ_6, chosen so that it leads to rich thermodynamics. It has been taken from [11],[1]:

$$V(\phi) = -\frac{4}{3}W(\phi)^2 + \frac{1}{2}W'(\phi)^2 \tag{2.2}$$

$$LW(\phi) = -\frac{3}{2} - \frac{\phi^2}{2} + \lambda_4\phi^4 + \lambda_6\phi^6 \tag{2.3}$$

This potential has a maximum at $\phi = 0$ and for certain values of λ_4 and λ_6 it will also have a minimum at $\phi = \phi^*$. We will be working with $\lambda_6 > 0$, so this minimum will always exist.

$$\phi^* = \sqrt{\frac{1}{2\lambda_4 + \sqrt{4\lambda_4^2 + 6\lambda_6}}} \tag{2.4}$$

This maximum will correspond to the UV limit while the minimum will correspond to the IR limit. Since they are extrema they will both correspond to CFTs. To explore the UV limit we can expand the potential around $\phi = 0$

$$L^2V(\phi) = -3 - \frac{3\phi^2}{2} - \frac{\phi^4}{3} + \left(8\lambda_4^2 + \frac{4\lambda_4}{3} - 2\lambda_6\right)\phi^6 + O\left(\phi^7\right) \tag{2.5}$$

This will correspond to a UV fixed point, and from the quadratic term in the potential it can be seen that the field will have a mass of $m_{UV}^2 = -3/L^2$. This means that the field has a conformal dimension $\Delta_{UV} = 3$, found through $m_{UV}^2 = \Delta_{UV}(\Delta_{UV} - d)$. This means that the scalar field will correspond to a relevant operator which will drive the RG flow away from the fixed point.

Since at the IR limit $\phi \to \phi^*$ there is a minimum m_{IR}^2 must be positive, and using $m_{IR}^2 = \Delta_{IR}(\Delta_{IR} - d)$ this means that it will have a conformal dimension $\Delta_{IR} > d$. So at the IR limit the scalar field will correspond to an irrelevant operator.

This action and potential yield the following equations of motion for the metric and the scalar field:

$$\frac{1}{\sqrt{-G}}\partial_N\left[\sqrt{-G}G^{MN}\partial_M\phi\right] = \partial_\phi V(\phi) \tag{2.6}$$

$$\mathcal{R}_{MN} - \frac{1}{2}\mathcal{R}G_{MN} = \frac{\kappa_5^2}{4}T_{MN} \tag{2.7}$$

Where the stress-energy tensor is given by:

$$T_{MN} = \frac{4}{\kappa_5^2}\left[2\partial_M\phi\partial_N\phi - G_{MN}\left(G^{AB}\partial_A\phi\partial_B\phi + 2V(\phi)\right)\right] \tag{2.8}$$

2.1 Holographic renormalization

Next we want to obtain the stress-energy tensor at the boundary to get the observables of the QFT such as the energy or the pressures, but our stress-energy tensor diverges at the boundary. To solve this we will use the well-known holographic renormalization procedure from [6],[5]. Holographic renormalization is usually implemented using Fefferman Graham (FG) coordinates for AdS_5. Near the boundary the metric behaves as:

$$ds^2 = \frac{L^2}{z^2}dz^2 + g_{\mu\nu}dx^\mu dx^\nu \tag{2.9}$$

with:

$$g_{\mu\nu} = g_{\mu\nu}^{(0)}(t,\vec{x}) + g_{\mu\nu}^{(2)}(t,\vec{x})z^2 + g_{\mu\nu}^{(4)}(t,\vec{x})z^4 + \cdots; \tag{2.10}$$

while the scalar decays as

$$\phi = \phi^{(0)}(t,\vec{x})z + \phi^{(2)}(t,\vec{x})z^3 + \cdots. \tag{2.11}$$

Higher order terms in the expansion are determined in terms of these.

In general $g_{\mu\nu}^{(i)}$ and $\phi^{(i)}$ depend on all the gauge theory coordinates, but in this project we will restrict $g_{\mu\nu}^{(0)}$ to the flat Minkowski metric, while $\phi^{(0)}(t,\vec{x}) = \phi_0 = \Lambda$ is constant and identified as the source of the operator dual that breaks conformal symmetry at the UV. This also fixes $g_{\mu\nu}^{(2)} = -\Lambda^2 L^2 g_{\mu\nu}^{(0)}/3$, making $g_{\mu\nu}^{(4)}(t,\vec{x})$ and $\phi^{(2)}(t,\vec{x})$ the only functions left undetermined.

Since our boundary metric is conformally flat and we have a constant source for our scalar field the expressions from ([6]) will be dramatically simplified. The vacuum expectation value of the energy-momentum tensor reads ([2])

$$\langle T_{\mu\nu} \rangle = \frac{2L^3}{\kappa_5^2} \left[g_{\mu\nu}^{(4)}(t, \vec{x}) + g_{\mu\nu}^{(0)} \Lambda \phi^{(3)}(t, \vec{x}) - \frac{\Lambda^4}{18} + \lambda_4 \phi_1^4 \right] . \tag{2.12}$$

Similarly, the vacuum expectation value of the operator dual to ϕ is

$$\langle \mathcal{O}_\phi \rangle = \frac{2L^3}{\kappa_5^2} \left[-2\phi^{(3)}(t, \vec{x}) - 4\lambda_4 \Lambda^3 \right] \tag{2.13}$$

It is important to note that these expressions satisfy the Ward identity

$$\left\langle T^\mu_{\ \mu} \right\rangle = -\Lambda \langle \mathcal{O} \rangle , \tag{2.14}$$

2.2 Homogeneous Setup

We still have to implement some conditions on the boundary metric, which will dictate how the theory behaves. The first case we want to study is one in which the system will relax towards an equilibrium state. To do so we will force all observables to only depend on time, making all solutions homogeneous. This will mean that there cannot be any $q \neq 0$ momentum modes and thus no hydrodynamic modes will be excited. This setup can be useful to find equilibrium solutions or compute quasi-normal modes, as we will see later.

Also the fact that all observables only depend on time means that the equations will only depend on the holographic coordinate z and on t, simplifying the resolution.

2.3 Boost Invariant Setup

If we want to allow hydrodynamic modes to appear we must allow the plasma's properties to depend not only on time but also one spatial direction, which we will call the longitudinal coordinate x_L. To do se we will work in new coordinates, where instead of

using time t and x_L we will use proper time τ and rapidity y. They are related as:

$$t = \tau \cosh(y) \quad x_L = \tau \sinh(y), \tag{2.15}$$

and the metric reads:

$$ds^2 = -d\tau^2 + \tau^2 dy^2 + d\mathbf{x}_T^2 \tag{2.16}$$

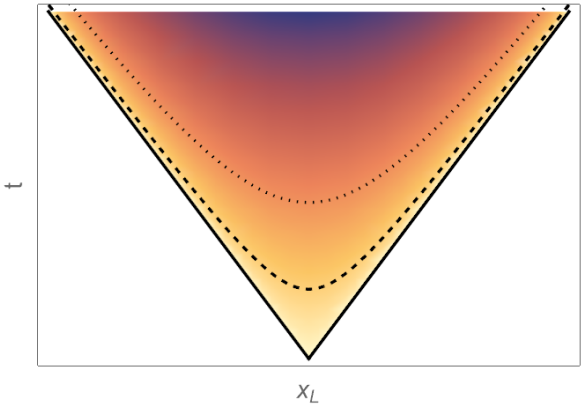

Figure 1: Diagram of the boost invariant setting. The thick black line corresponds to $\tau = 0$, where the energy density diverges. The dashed line corresponds to τ_{ini} where our simulation begins, and the dotted one corresponds to τ_{hydro} when the system will hydrodynamize.

And we will require the metric and all properties of the plasma to only depend on τ and be invariant on rapidity, hence the name. This was first proposed by Bjorken [7] more than thirty years ago for a conformal case which can be solved analitically [14],[13]. We will also study it numerically in the non conformal case.

The motivation for this assumption comes from heavy ion collisions. While no collision with finite energy can have a homogeneous rapidity distribution from $-\infty$ to ∞, we could expect that at high energies the stress-energy tensor of the fluid is independent of y over some finite range, and this would mean that after hadronization the profile would have a wide plateau. Then in high energy limit the plateau would become an homogeneous spectrum over y and we would be in the boost invariant regime. However it has been found from heavy ion collisions at RHIC that the rapidity profile does not show a plateau, but rather a gaussian distribution [17].

One can then wonder about the applicability of this model, but it will be useful as a simple model to study how a system initially far from equilibrium can hydrodynamize as it expands and cools.

In this case energy density is not constant due to the plasma being forced to expand. Also, at $\tau = 0$ there is a coordinate singularity and the energy density diverges, which means that all our simulations will start at some initial time τ_{ini}. Then they will cool down until the system becomes well described by hydrodynamics as seen in (Fig 1). Since all functions only depend on τ we will again have equations of motion which will only depend on two variables and we will solve them with a similar scheme as in the homogeneous setup.

3 Thermodynamics and transport

We now want to explore the thermodynamics and transport coefficients of the system, and to do so we solve the equilibrium solutions of the metric (2.9).

3.1 Static solutions

We assume that the equilibrium state will be homogeneous, isotropic and static, and therefore we propose the following ansatz:

$$ds^2 = \frac{L^2}{z^2}\left(-f(z)dt^2 + g(z)d\mathbf{x}^2 + dz^2\right) \tag{3.1}$$

The boundary metric will be conformal to Minkowski, which will fix the boundary behaviour of the metric coefficients.

Next we can plug our metric ansatz into Einstein's equations (2.6), which yields two coupled second order differential equations for $g(z)$ and $\phi(z)$ and a first order differential equation for $f(z)$.

$$\begin{aligned} \frac{z^2 g''}{g} - \frac{3zg'}{g} + \frac{z^2\phi'^2}{6} + \frac{L^2 V}{3} &= 0, \\ z^2\phi'' - \left[1 - \frac{zg'}{g} - \frac{g(z^2\phi'^2 - 2L^2V)}{6z^3(g/z^2)'}\right] z\phi' - L^2\partial_\phi V &= 0, \\ \frac{zf'}{f} + \frac{zg'}{g} - \frac{g(z^2\phi'^2 - 2L^2V)}{3z^3(g/z^2)'} - 4 &= 0. \end{aligned} \tag{3.2}$$

What we will do to solve these equations is study how the functions must behave close to the event horizon of the black hole, and numerically integrate outward towards the boundary. From regularity conditions we can find that near the horizon the metric functions must behave as:

$$\begin{aligned} f(z) &= f_H(z - z_H)^2 + \mathcal{O}(z - z_H)^3 \\ g(z) &= g_H + \mathcal{O}(z - z_H) \\ \phi(z) &= \phi_H + \mathcal{O}(z - z_H) \end{aligned} \tag{3.3}$$

Now we can do a series expansion of our field equations near the horizon, and solve them order by order. Then we can express the expansion for the three functions in terms of f_H,

g_H and ϕ_H, and we get:

$$\begin{aligned} f(z) &= f_H(z-z_H)^2 + \frac{f_H(z-z_H)^3}{z_H} + \frac{f_H(z-z_H)^4\left(8L^2V(\phi_H)-3\right)}{36z_H^2} + \mathcal{O}(z-z_H)^5 \\ g(z) &= g_H + \frac{2g_H(z-z_H)}{z_H} - \frac{g_H(z-z_H)^2\left(2L^2V(\phi_H)-3\right)}{3z_H^2} + \mathcal{O}(z-z_H)^3 \\ \phi(z) &= \phi_H + \frac{L^2(z-z_H)^2V'(\phi_H)}{4z_H^2} - \frac{L^2(z-z_H)^3V'(\phi_H)}{4z_H^3} + \mathcal{O}(z-z_H)^4 \end{aligned} \tag{3.4}$$

And so it seems that our solutions will be parameterized by these three variables plus the position of the horizon z_H. But in the homogeneous case we expect the equilibrium state to be determined only by one parameter, the energy. Later we will see how three of these will get fixed, and thus the equilibrium solutions will be given by just one parameter ϕ_H

Next let us study how the metric must behave near the boundary $z = 0$. Since we are dealing with a homogeneous plasma, the boundary metric should be conformal to Minkowski. Imposing (3.1) to be Minkowski at the boundary means that the values for $f(z)$ and $g(z)$ at $z = 0$ are $f(0) = g(0) = 1$. Looking at the near expansion of the scalar field in (**??**) $\phi(z)$ should behave as $\phi(z) = z\Lambda + z^3\phi_2 + \mathcal{O}(z)^4$, where Λ is the source of the scalar field and ϕ_2 is a free parameter not given by the expansion. And if we then solve the equations order by order near the boundary we find:

$$\begin{aligned} f(z) &= 1 - \frac{1}{3}z^2\Lambda^2 + f_4 z^4 + \mathcal{O}\left(z^5\right) \\ g(z) &= 1 - \frac{1}{3}z^2\Lambda^2 + \frac{1}{27}z^4\left(-9f_4 + 2\Lambda^4 - 18\phi_2\Lambda\right) + \mathcal{O}\left(z^5\right) \\ \phi(z) &= z\Lambda + z^3\phi_2 + \mathcal{O}\left(z^5\right) \end{aligned} \tag{3.5}$$

where we have two coefficients that are not determined by the equations f_4, ϕ_2. Now we want to integrate the equations of motion (3.2) from the horizon up to the boundary in order to find the whole profile of our fields. But we run into the problem that our equations are singular at the horizon, and so we will use the near horizon expansion up to sufficient high order to evaluate the equations at some small ε_{IR} close to the horizon. From there we can integrate upwards towards the boundary, but again the equations are singular there so we will integrate up to a cut-off ε_{UV} close to the boundary. We have also checked the stability of the solutions under changes of ε_{IR} and ε_{UV}. Now one would think that the system is solved, but we do not know if the behave as we want around the

boundary.

And indeed by integrating the equations with an arbitrary choice for the coefficient values at the horizon we find that they do not have the required boundary conditions. This is clearly a problem, caused by having too many free parameters, f_H, g_H, z_H and ϕ_H. We can solve this by realising that Einstein's equations are invariant under the following changes:

$$\begin{aligned} f(z) &\to \alpha\ f(z) \\ g(z) &\to \beta\ g(z) \\ z &\to \gamma\ z \end{aligned} \tag{3.6}$$

This means that we have three conditions to fix on the boundary, $f(0) = g(0) = 1$ and $\phi'(0) = 1$ to measure everything in units if Λ. And so what we will do is start by integrating from the horizon with some chosen values for $f_H = g_H = z_H = 1$ and the desired one for ϕ_H. We will get the values for these functions at the boundary, and from them compute $\alpha = f(0)^{-1}$, $\beta = g(0)^{-1}$ and $\gamma = \phi'(0)$. Finally using (3.6) we can compute the new values for f_H, g_H, z_H and again integrate to the boundary, where now the conditions will be automatically satisfied.

Since the only value which remains unfixed is ϕ_H, this means that our equilibrium solutions will only be given by one parameter, which will relate to the energy and temperature of the system. As we said before the potential $V(\phi)$ has a maximum at $\phi = 0$ and a minimum at ϕ_*, and our solutions will be given by $\phi_H \in (0, \phi_*)$. $\phi_H \to 0$ will correspond to the high energy limit while $\phi_H \to \phi_*$ to the low energy limit.

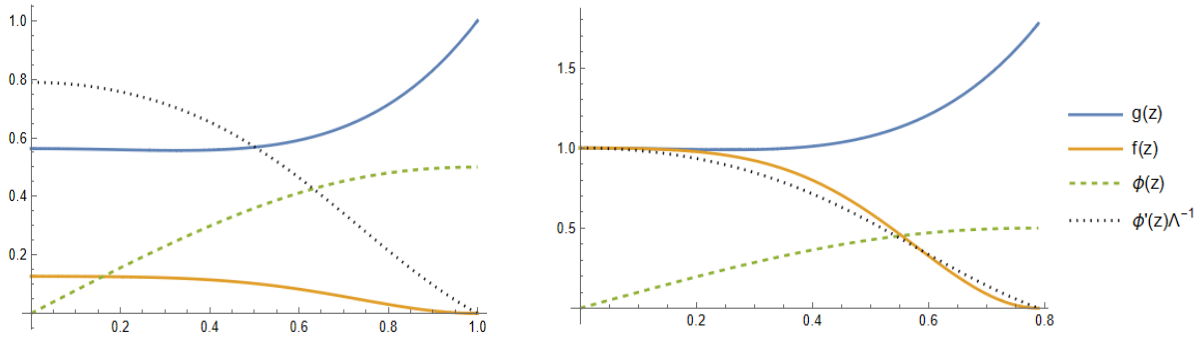

(a) **(b)**

Figure 2: Profiles for $g(z)$, $f(z)$, $\phi(z)$, and $\phi'(z)$, before (a) and after (b) making the transformation (3.6). As can be seen in the right picture all boundary conditions are satisfied.

3.2 Thermodynamics

For the case of our static metric with the expansions from (3.5) we get the following expressions for energy and pressure from holographic renormalization (2.12).

$$\epsilon \equiv T_t{}^t = -f_4 - \lambda_4 \Lambda^4 + \frac{\Lambda^4}{18} - \Lambda\phi_2 \tag{3.7}$$

$$P \equiv T_x{}^x = \frac{1}{54}\left(-18 f_4 + 54\lambda_4\Lambda^4 + \Lambda^4 + 18\Lambda\phi_2\right) \tag{3.8}$$

Now that we have the energy and the pressure we need to get the other thermodynamic variables, the temperature and entropy. They will both be obtained through black hole thermodynamics.

3.2.1 Temperature

As proved by Stephen Hawking [12], in black hole thermodynamics temperature is usually described in terms of the surface gravity κ. Here though we will compute it using imaginary time. If we focus only on the dz, dt part of the metric:

$$ds^2 = \frac{L^2}{z^2}\left(dz^2 - f(z)dt^2\right) \tag{3.9}$$

Since the temperature is defined at the horizon we can make an expansion around z_H, where we obtain:

$$ds^2 = \frac{L^2}{z_H^2}\left(dz^2 - f_H(z - z_H)^2 dt^2\right) \tag{3.10}$$

And if we make a coordinate transformation $z \to \rho + z_H$:

$$ds^2 = \frac{L^2}{z_H^2}\left(d\rho^2 - f_H \rho^2 dt^2\right) \tag{3.11}$$

Now we can go to imaginary time, a trick from statistical physics where we perform the transformation $t \to -i\tau$ that brings us to an euclidian metric. This new coordinate will be periodic $\tau \sim \tau + \beta$, where β is related to the temperature by $\beta = \frac{1}{T}$.

$$ds^2 = \frac{L^2}{z_H^2}\left(d\rho^2 + f_H \rho^2 d\tau^2\right) \tag{3.12}$$

We want to avoid conical singularities, which means we need the metric to be equivalent to:

$$ds^2 = \frac{L^2}{z_H^2}\left(d\rho^2 + \rho^2 d\phi^2\right) \tag{3.13}$$

with $\phi \in (0, 2\pi)$. Therefore $f_H \beta^2 = (2\pi)^2$, and the temperature can be expressed as:

$$T = \frac{\sqrt{f_H}}{2\pi} \tag{3.14}$$

3.2.2 Entropy

On the other hand, the entropy density is given in terms of the area of the black hole by the Bekenstein Hawking formula [4]:

$$S = \frac{A}{4G_5} = \frac{8\pi A}{\kappa_5^2} \tag{3.15}$$

In this metric the space coordinates perpendicular to the event horizon $x_L, \mathbf{x}_T$ are not compact, so the area itself will diverge. The timeslice perpendicular to the horizon will be when $dt = 0$, $dz = 0$, so the resulting induced metric γ_{ij} will be:

$$ds^2 = \frac{L^2}{z^2} g(z) d\mathbf{x}^2 \tag{3.16}$$

Since the area of the black hole diverges we will work with an area density and thus compute the entropy density. This area density will be given by square root of the

determinant of the spatial component of the metric, $\sqrt{Det(\gamma_{ij})} = \frac{L^3}{z_H^3} g^{3/2}(z)$. Then this finally means that the entropy density is given by:

$$s = \frac{dS}{dx_L dx_T^2} = \frac{8\pi L^3 g^{3/2}(z_H)}{\kappa_5^2 z_H^3} \tag{3.17}$$

Or expressing it the same units as in (2.12) we obtain:

$$s = \frac{L^3}{2\kappa_5^2} \frac{4\pi g_H^{3/2}}{z_H^3} \tag{3.18}$$

3.3 Results

And so now given a value for λ_4 and λ_6, which from now on we will set as $\lambda_6 = 1/10$, we can compute the full metric solutions for different values of $\phi_H \in (0, \phi^*)$, and get the thermodynamic structure of the system. For example we can plot the equation of state of the system $3P/\epsilon$ and the ratio s/T^3 as a function of temperature.

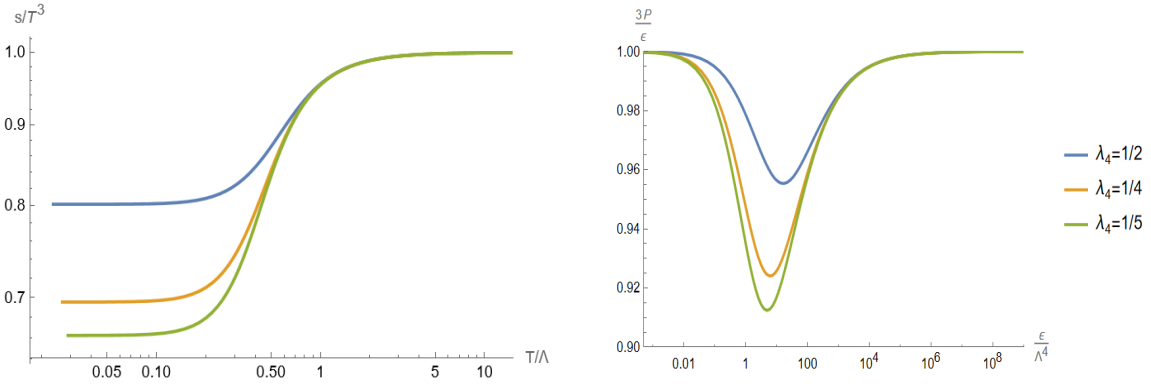

(a) **(b)**

Figure 3: Ratio of s/T^3 and equation of state as a function of temperature for different values of λ_4.

From these pictures we can indeed check that our theory tends to a CFT in the high and low energy limits. In a CFT the energy momentum tensor is traceless, which immediately implies the equation of state $P(\epsilon) = \epsilon/3$. Also since the ratio s/T^3 it will be constant constant in a CFT, and looking at figure 3) we can see that at high energies they all tend towards the same value, while at low values the ratio goes to different limits depending

on λ_4.

As explained in [2], the ratio s/T^3 is related to the effective degrees of freedom of the theory, which means that at the UV all theories converge to the same CFT, which makes sense since there $\phi \to 0$. On the other hand in the IR they flow to CFTs with different effective degrees of freedom.

But we want to make sure our results are correct, so we will make one numerical check. Given the thermodynamical identity $s = \frac{-df}{dT}$, we can compare the results for the entropy obtained from the free energy to those obtained through black hole thermodynamics (3.18).

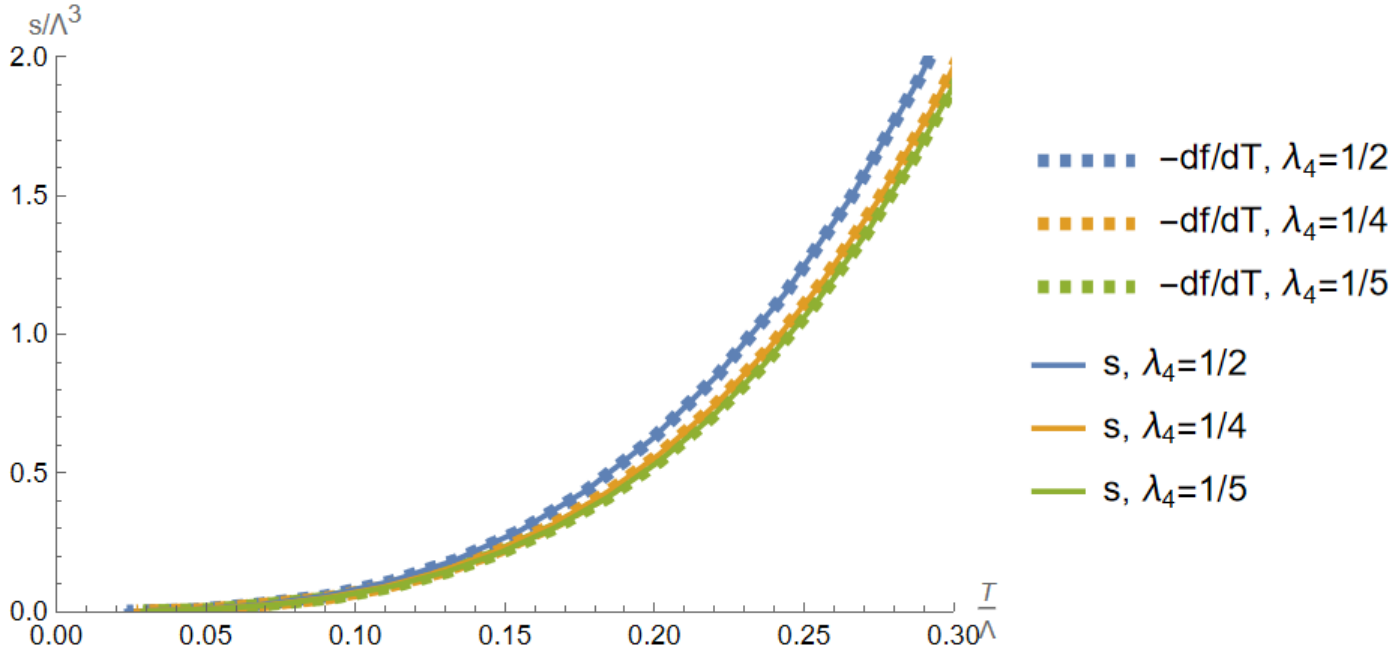

Figure 4: Comparison between the derivative of the pressure with respect to the temperature and the entropy, which as can be seen overlap.

3.4 Phase Diagram

The superpotential (2.3) has some thermodynamic richness we have yet to study, since so far we have only looked at the solutions when $\lambda_4 > 0$. If we study the free energy f as a function of temperature we find that for certain values of λ_4 the free energy is multi-valued, signaling the presence of a first order phase transition. We can also clearly see it when plotting energy as a function of temperature where the characteristic "s" shape of a first order phase transition appears.

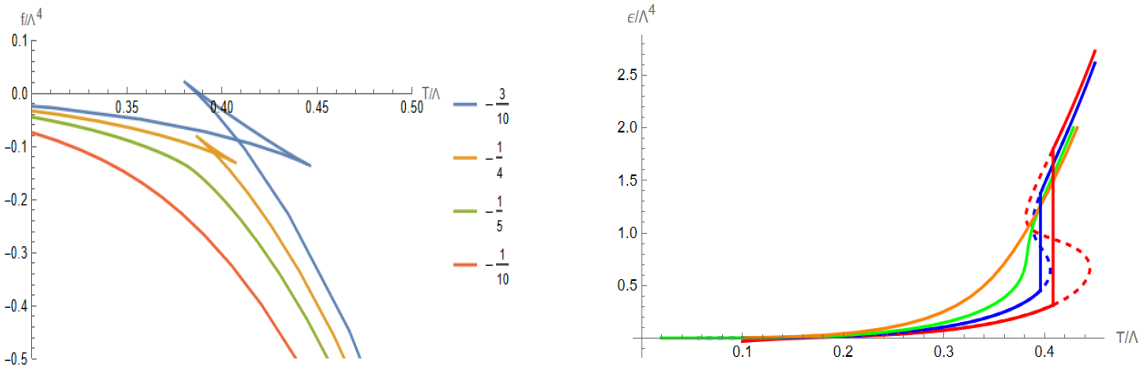

(a) **(b)**

Figure 5: Free energy (a) and energy (b) as a function of temperature for different values of λ_4. As the value of λ_4 decreases a first order phase transition starts appearing.

And so what we find is that for $\lambda_4 \in (-\infty, \lambda_c)$ there is a first order phase transition characterised by the free energy being multivalued with two unstable branches, and with the critical temperature T_c being at the point where these branches meet. At $\lambda_4 = \lambda_c$ the free energy stops being multivalued but its derivative is still discontinuous, so we find ourselves at a second order phase transition. For values of λ_4 closer to zero the free energy goes through a smooth crossover, and there is no longer a phase transition.

To find the critical temperature we study the free energy and find when the first branch ends and where the second one begins, characterized by the two flips in the sign of $T'(\epsilon)$. We then interpolate both branches numerically and see where they both meet. This will be the critical temperature T_c. We can do this for various values of λ_4 until we see that the free energy is no longer multivalued. We can make more fine changes to λ_4 around that region to find the value λ_c that separates the two behaviours, which will correspond to the second order phase transition.

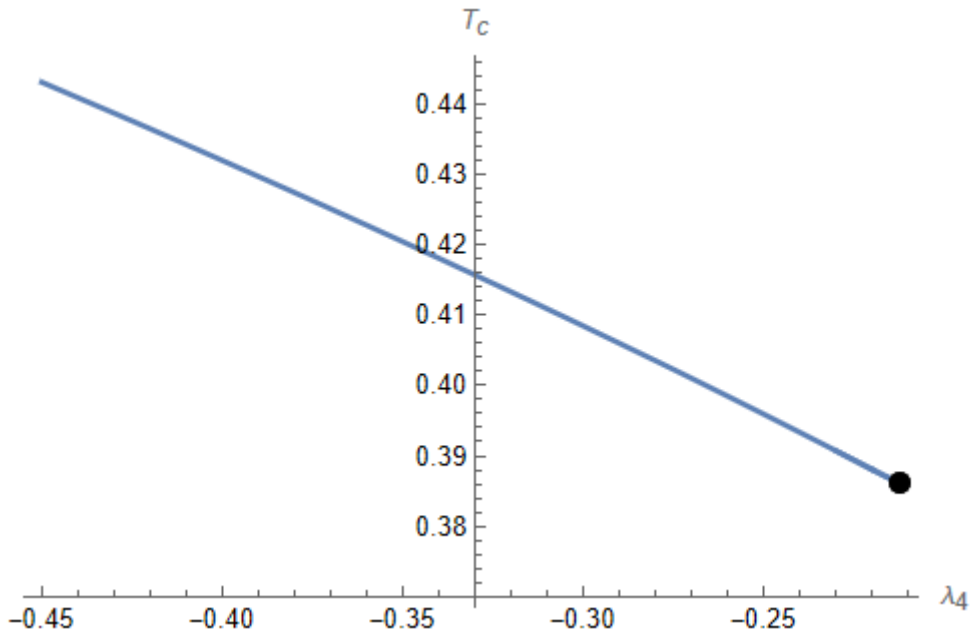

Figure 6: Critical temperature as a function of the parameter λ_4.

The value found for the critical parameter is $\lambda_c \approx 0.212 \pm 0.001$, which is in agreement with [11] where they find $\lambda_c \approx 0.21123$.

It is also interesting to study the speed of sound $c_s = \frac{s}{T}\frac{dT}{ds}$ along this phase transition, which dictates the stability of the system. When $c_s^2 < 0$ instabilities will be amplified and the system will be unstable, and as can be seen in figure 7 the region corresponding to the spinodal branch is unstable. We will talk more about this and its implications when we run the dynamical evolutions.

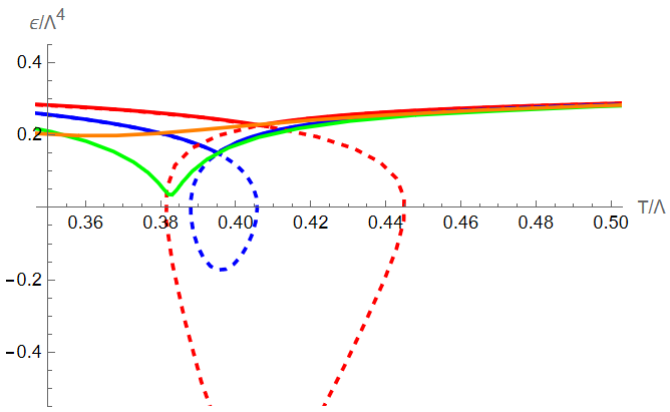

Figure 7: Speed of sound c_s as a function of temperature

3.5 Transport coefficients

Later we will want to study the hydrodynamic behaviour of the plasma, and to do that we will need to compute the shear and bulk viscosities η and ζ. Let us start with the shear viscosity. all theories with a two derivative gravity dual obey $\eta/s = 1/4\pi$ [8], both in the conformal and non-conformal case. This makes it easy to compute, since we already know the expression for the entropy.

The bulk viscosity on the other hand is obtained from the variation of the entropy with respect to the value of the field at the horizon ϕ_H [10]:

$$\frac{\zeta}{\eta} = 4\left(\frac{d\log s}{d\phi_{\mathrm{H}}}\right)^{-2} \tag{3.19}$$

$$\frac{\eta}{s} = \frac{1}{4\pi} \tag{3.20}$$

$$\lambda_c \approx 0.212 \tag{3.21}$$

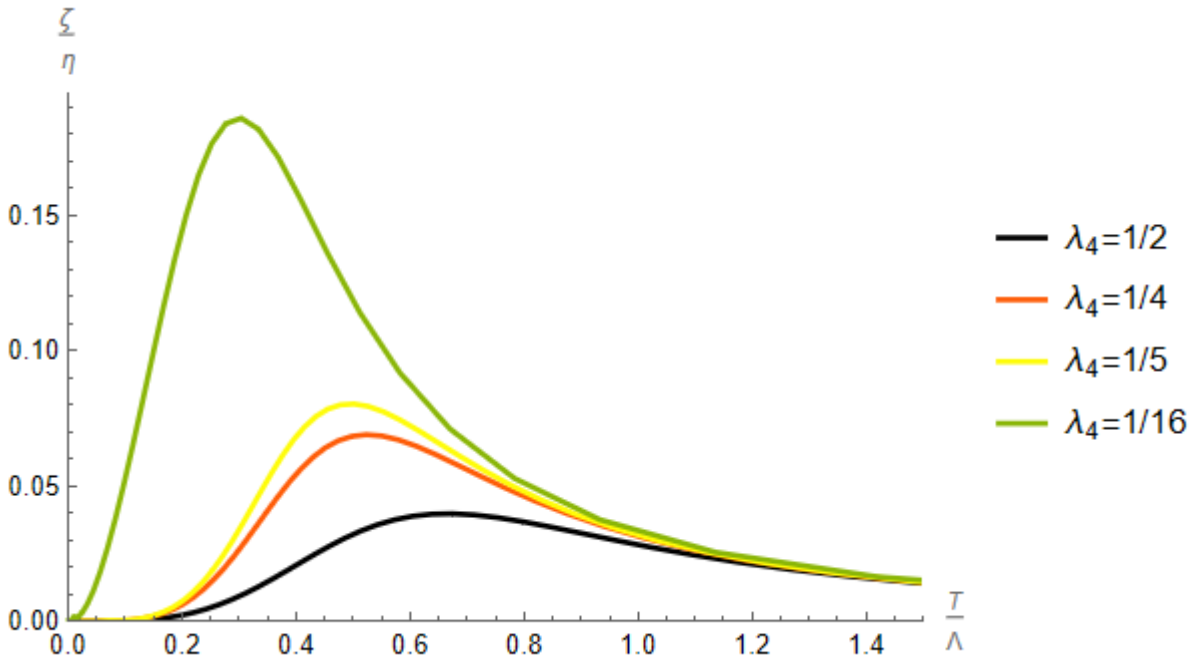

Figure 8: Ratio of bulk and shear viscosity as a function of temperature. As can be seen at high and low energies the ratio approaches 0, since in a CFT ζ is negligible compared to other magnitudes.

4 Hydrodynamics

Out of equilibrium systems can be hard to describe, but hydrodynamics gives us a tool to compute the evolution of its near equilibrium properties. Whenever the evolution of a system is slow in time and space compared to a certain microscopic scale, hydrodynamics applies. We will use relativistic hydrodynamics, which is useful for astrophysics, heavy ion collisions and cosmology.

The fields we will use to describe our system are the energy density ϵ and the local four velocity of the fluid u^μ. We will also be working in the boost invariant setup we have described before, where the four velocity is $u^\mu = (1, 0, 0, 0)$ and the metric is

$$ds^2 = -d\tau^2 + \tau^2 dy^2 + d\mathbf{x}_T^2. \tag{4.1}$$

We are using this setup since we want to describe heavy ion collisions, and generalise the Bjorken flow to non-conformal theories. If we work up to first order in the hydrodynamic expansion, the stress energy tensor has the following form [3]:

$$T^{\mu\nu} = \epsilon u^\mu u^\nu + p\Delta^{\mu\nu} - \eta\sigma^{\mu\nu} - \zeta\Delta^{\mu\nu}\nabla_\alpha u^\alpha. \tag{4.2}$$

Where $\Delta^{\mu\nu} = g^{\mu\nu} + u^\mu u^\nu$ is the projector onto the space transverse to the local velocity, $u_\mu \Delta^{\mu\nu} = 0$. The shear tensor is

$$\sigma^{\mu\nu} = \Delta^{\mu\alpha}\Delta^{\nu\beta}(\nabla_\alpha u_\beta + \nabla_\beta u_\alpha) - \frac{2}{3}\Delta^{\mu\nu}\nabla_\lambda u^\lambda. \tag{4.3}$$

It is defined in this way such that it is traceless and transverse, $\sigma^\mu{}_\mu = 0$, $u_\mu \sigma^{\mu\nu} = 0$.

If we now plug the expression for u^μ into the stress energy tensor (4.2) we find that the energy momentum tensor will have three independent non-vanishing components:

$$\begin{aligned} \epsilon &\equiv -T_\tau{}^\tau \\ P_L &\equiv T_y{}^y = P - \frac{1}{3\tau}(4\eta + 3\zeta) \\ P_T &\equiv T_{x_T}{}^{x_T} = P + \frac{1}{3\tau}(2\eta - 3\zeta) \end{aligned} \tag{4.4}$$

which we will refer to as energy, longitudinal pressure and transverse pressure respectively.

But to obtain how these values evolve over time we must use the conservation equation $\nabla_\mu T^{\mu\nu} = 0$ and the equation of state $P(\epsilon)$.

4.1 Bjorken Flow

Let us start with finding the time evolution of the system for the conformal case where the trace of the energy momentum tensor vanishes, $T^\mu_{\ \mu} = 0$. This means that:

$$P(\epsilon) = \frac{\epsilon}{3} \tag{4.5}$$

$$\zeta(\epsilon) = 0 \tag{4.6}$$

Using the conservation equation and allowing for the shear viscosity to depend on time we obtain:

$$-P(\tau) + \frac{4\eta(\tau)}{3\tau} - \tau\epsilon'(\tau) - \epsilon(\tau) = 0 \tag{4.7}$$

At late times the term belonging to $\eta(t)$ will be negligible, so the equation will be:

$$\tau\epsilon'(\tau) - \frac{4}{3}\epsilon(\tau) + \mathcal{O}(\tau^{-1}) = 0 \tag{4.8}$$

And has a simple solution for the energy density, $\epsilon(\tau) = C\tau^{-4/3}$, where C is a integration constant that determines the energy scale. To include the viscous terms and go to second order we need to know how η scales with energy, and as we explained earlier $\eta/s = 1/4$. According to [3] we can express it as:

$$\eta(\epsilon) = C\eta_0 \left(\frac{\epsilon}{C}\right)^{3/4}, \tag{4.9}$$

with $\eta_0 = \frac{1}{3\pi}$. Now we can solve the whole differential equation, obtaining:

$$\epsilon(\tau) = C\left(\frac{1}{\tau^{4/3}} - \frac{2\eta_0}{\tau^2}\right) \tag{4.10}$$

And the pressures behave as follows:

$$\begin{aligned} P_L &= \frac{C}{3\tau^{4/3}} - \frac{2C\eta_0}{\tau^2} \\ P_T &= \frac{C}{3\tau^{4/3}} \end{aligned} \tag{4.11}$$

Since at low energies our theory flows into a CFT, we expect that at late times the energy and pressures will behave in this way.

4.2 Non Conformal Flow

But our system has a scalar field that breaks conformality, so the Bjorken flow will only apply at very late times when we are in the IR limit. In the general non-conformal case the equation of state is analitically unknown, so we will not be able to solve the conservation equations as before.

To get the equation of state we will use our static solutions code, where we find a relation $P(\epsilon) = \omega(\epsilon)\epsilon$. We have also computed numerical expressions for the transport coefficients $\eta(\epsilon)$ and $\zeta(\epsilon)$, and from (4.11) we have a prediction for $P_L(\tau, \epsilon)$ and $P_T(\tau, \epsilon)$, which we can compare to a dynamical simulation.

But it is important to note that this does not tell us how energy will evolve with time, to do that we need to solve the equation for the conservation of the energy momentum tensor. To do that we need to use the conservation equation $\nabla_\mu T^{\mu\nu} = 0$, which can be expressed as

$$-P(\epsilon(\tau)) + \frac{4\eta(\epsilon(\tau)) + \zeta(\epsilon(\tau))}{3\tau} - \tau\epsilon'(\tau) - \epsilon(\tau) = 0 \tag{4.12}$$

This equation can now be solved numerically to obtain a profile for $\epsilon(\tau)$, and consequently for the shear and bulk viscosities and the longitudinal and transverse pressures. What should be done is start at a late time and low energy state when we expect hydrodynamics to be a good description of the system, and integrate the equation backwards to get a profile of $\epsilon(\tau)$ which should match the simulation up to a certain τ where hydrodynamics no longer applies. However this was outside the scope of this project, and would be interesting to compute it in the future.

5 Dynamical Evolution

5.1 Eddington Finkelstein Coordinates

To solve the numerical evolution we will be working with a metric ansatz for AdS_5 in Eddington Finkelstein coordinates (EF).

$$ds^2 = 2drdt - A(r,t)dt^2 + S(r,t)^2 e^{-2B(r,t)} dx_L^2 + S(r,t)^2 e^{B(r,t)} d\mathbf{x}_T^2 \tag{5.1}$$

In this metric r is the radial holographic coordinate, where now the boundary is at $r = \infty$, and x_L and x_T are the longitudinal and transversal coordinates respectively. They are called so because the collisions and expansions of the plasma will be along the longitudinal coordinate. The boundary of the AdS_5 is at $r \to \infty$, and there we will impose a boundary metric depending on the kind of setup we want to use.

We are using this metric because as we will see later it will let us work along null ingoing geodesics, allowing us to solve Einstein's equations.

5.1.1 Gauge Symmetry

The metric in Eddington Finkelstein coordinates has a gauge symmetry which will become really important later on. If we perform the change of coordinates $r \to r + \xi(t)$ the metric transforms as:

$$ds^2 = 2drdt + 2\partial_t \xi(t) dt^2 - \bar{A}(r,t)dt^2 + \bar{S}(r,t)^2 e^{-2\bar{B}(r,t)} dx_L^2 + \bar{S}(r,t)^2 e^{\bar{B}(r,t)} d\mathbf{x}_T^2, \tag{5.2}$$

And if the metric coefficients transform as $A \to \bar{A} = A + 2\partial_t \xi$, $S \to \bar{S} = S$ and $B \to \bar{B} = B$ the metric will remain invariant. This means that the metric will be free under shifts of the holographic radial coordinate without affecting any of the physics or the observables. Later we will explain how to fix this gauge symmetry.

5.2 Characteristic Einstein Equations

The advantage of using EF coordinates (5.1) is that the evolution equations can be written in a nested form by changing the time derivatives into derivatives along null ingoing

geodesics and using derivatives along the holographic radial direction. [9]

$$\dot{f} = \partial_t f + \frac{1}{2} A \partial_r f \tag{5.3}$$

$$f' = \partial_r f \tag{5.4}$$

By doing so we obtain:

$$\begin{aligned}
S'' &= -\frac{1}{6} S \left(3 \left(B' \right)^2 + 4 \left(\phi' \right)^2 \right) \\
S \dot{S}' &= -\frac{2}{3} \left(S^2 V(\phi) + 3 \dot{S} S' \right) \\
2 S \dot{B}' &= -3 \left(\dot{S} B' + \dot{B} S' \right) \\
2 S \dot{\phi}' &= S \partial_\phi V(\phi) - 3 \left(\dot{\phi} S' + \dot{S} \phi' \right) \\
S^2 A'' &= S^2 \left(-3 \dot{B} B' + \frac{4 V(\phi)}{3} - 4 \dot{\phi} \phi' \right) + 12 \dot{S} S' \\
\partial_t \dot{S} &= \frac{1}{6} \left(3 \dot{S} A' - S \left(3 \dot{B}^2 + 4 \dot{\phi}^2 \right) \right)
\end{aligned} \tag{5.5}$$

These equations have a clearly nested structure, and by having the initial profiles for $B(z, t_i)$ and $\phi(z, t_i)$, they all become first or second order ordinary differential equations that can be easily solved to find S, $\dot{S}$, $\dot{B}$, $\dot{\phi}$, A and $\partial_t \dot{S}$. The last equation is a constraint equation and thus should always vanish, but its deviations from zero will tell us about the precision of our numerics.

One difficulty with these equations is that as it will be seen in the next subsection the functions A and S both diverge at the boundary $r = \infty$, which means that all the equations will diverge too. Thus we will have to redefine our fields to work with finite variables.

5.2.1 Near Boundary Expansion

We want to study how the functions behave near the boundary at $r = \infty$, which is where divergences will appear. Since we fix the boundary metric to be conformal to Minkowski, we can find how the metric functions should behave. By performing a Taylor expansion of these functions in r around the boundary, we can solve the equations of motion order by order in r and get the values of these coefficients. We will start by describing the procedure for the homogeneous case, and then we will tackle the boost invariant case.

Now we will perform a Taylor expansion of these functions in r, $A(r,t) = \sum_{n=0} A_n(t) r^{2-n}$.

If we solve the equations of motion order by order in r, we can get the values of these coefficients.

$$\begin{aligned}
A(r,t) &= r^2 + r\mathrm{A}_1(t) + \left(-\mathrm{A}_1'(t) + \frac{1}{4}\mathrm{A}_1(t)^2 - \frac{2\Lambda^2}{3}\right) + \frac{a_4(t)}{r^2} + \mathcal{O}\left(\frac{1}{r}\right)^3 \\
B(r,t) &= \frac{b_4(t)}{r^4} + \mathcal{O}\left(\frac{1}{r}\right)^5 \\
S(r,t) &= r + \frac{\mathrm{A}_1(t)}{2} - \frac{\Lambda^2}{3r} + \frac{\Lambda^2\mathrm{A}_1(t)}{6r^2} + \frac{\Lambda^4 - 18\Lambda\phi_2(t)}{54r^3} + \mathcal{O}\left(\frac{1}{r}\right)^4 \\
\phi(r,t) &= \frac{\Lambda}{r} - \frac{\Lambda\mathrm{A}_1(t)}{2r^2} + \frac{\phi_2(t)}{r^3} + \mathcal{O}\left(\frac{1}{r}\right)^4
\end{aligned} \tag{5.6}$$

As we can see some parameters $a_4(t)$, Λ, $\phi_2(t)$ and $A_1(t)$ and $b_4(t)$ are left undetermined by this expansion. As we mentioned before Λ corresponds to the source of the scalar field, and the rest will depend on the initial conditions. But from the previous section we know that under the transformation $r \to r + \xi(t)$, S and B remain unchanged while $A \to A + 2\partial_t\xi$. To satisfy this we find that $A_1(t) = 2\xi(t)$.

From now on we will use the radial coordinate $z = 1/r$, for which the boundary lies at $z = 0$. This is useful since we are interested in the behaviour at the boundary, and we need the radial coordinate to be finite to run the numeric evolution.

So, to avoid running into singularities in our numerical procedure we will define some new functions which are finite at the boundary, and we will solve the equations of motion with respect to these new variables:

$$\begin{aligned}
B(z,t) &= z^4\mathrm{Bf}(z,t) \\
\phi(z,t) &= z^3\phi\mathrm{f}(z,t) - \frac{1}{2}\Lambda z(z\xi(t) - 2) \\
S(z,t) &= z^2\mathrm{Sf}(z,t) + \frac{\xi(t)}{2} - \frac{\Lambda^2 z}{3} + \frac{1}{z} \\
\dot{S}(z,t) &= z^2\dot{S}f(z,t) + \frac{3(z\xi(t)+2)^2 - 4\Lambda^2 z^2}{24z^2} \\
\dot{B}(z,t) &= z^3\dot{B}f(z,t) \\
\dot{\phi}(z,t) &= z^2\dot{\phi}f(z,t) - \frac{\Lambda}{2} \\
A(z,t) &= z^2\mathrm{Af}(z,t) - \frac{2\Lambda^2}{3} - \xi'(t) + \frac{(z\xi(t)+2)^2}{4z^2}
\end{aligned} \tag{5.7}$$

We will also need to set the boundary conditions for the differential equations, which come from comparing (5.7) with (5.6).

$$\begin{aligned}
\mathrm{Sf}(z,t)|_{z=0} &= \frac{1}{6}\Lambda^2\xi(t) \\
\dot{S}f(z,t)|_{z=0} &= \frac{1}{72}\left(36a_4(t) - 10\Lambda^4 - 9\Lambda^2\xi(t)^2 + 36\Lambda\phi_2(t)\right) \\
\dot{B}f(z,t)|_{z=0} &= -2b_4(t) \\
\dot{\phi}f(z,t)|_{z=0} &= \frac{1}{24}\left(8\Lambda^3 + 9\Lambda\xi(t)^2 - 36\phi_2(t)\right) \\
Af(z,t)|_{z=0} &= a4(t)
\end{aligned} \tag{5.8}$$

From this near boundary expansion we also find a constraint for $a4(t)$, which obeys:

$$\partial_t a4 = \frac{2}{3}\Lambda\left(\Lambda\xi(t)\xi'(t) - 2\phi_2'(t)\right) \tag{5.9}$$

Now we will do it for the boost invariant setup. Here the spatial coordinates are y and $\mathbf{x}_T$, and insted of time t we will be working with proper time. Since we want the metric at the boundary to be conformal to Minkowsi in these boost invariant coordinates the near boundary expansions are:

$$\begin{aligned}
A(r,\tau) &= r^2 + r\mathrm{Ac}_1(\tau) + \left(-\mathrm{Ac}_1'(\tau) + \frac{1}{4}\mathrm{Ac}_1(\tau)^2 - \frac{2j_1^2}{3}\right) + \frac{\mathrm{Ac}_4(\tau)}{r^2} + \mathcal{O}\left(\frac{1}{r}\right)^3 \\
B(r,\tau) &= -\frac{2\log(\tau)}{3} - \frac{2}{3r\tau} + \frac{\tau\mathrm{Ac}_1(t)+1}{3r^2\tau^2} + ... + \frac{\mathrm{Bc}_4(\tau)}{r^4} + \mathcal{O}\left(\frac{1}{r}\right)^5 \\
S(r,\tau) &= r\tau^{1/3} + \frac{3\tau\mathrm{Ac}_1(\tau)+2}{6\tau^{2/3}} - \frac{3j_1^2\tau^2+1}{9r\tau^{5/3}} + \frac{3j_1^2\tau^2\left(9t\mathrm{Ac}_1(\tau)-2\right)+9t\mathrm{Ac}_1(\tau)+10}{162r^2\tau^{8/3}} + \mathcal{O}\left(\frac{1}{r}\right)^3 \\
\phi(r,\tau) &= \frac{j_1}{r} - \frac{j_1\mathrm{Ac}_1(\tau)}{2r^2} + \frac{\phi\mathrm{c}_3(\tau)}{r^3} + \mathcal{O}\left(\frac{1}{r}\right)^4
\end{aligned} \tag{5.10}$$

And the finite functions will be:

$$
\begin{aligned}
B(z,\tau) &= z^4 \mathrm{Bf}(z,\tau) - \frac{6\left(6\tau^3\log(\tau) + z\left(6\tau^2 - 3\tau z + 2z^2\right)\right) + \tau z^2\left(8\Lambda^2\tau z + 9\xi(\tau)(\tau z\xi(\tau) - 2\tau + 2z)\right)}{54\tau^3} \\
\phi(z,\tau) &= z^3\phi\mathrm{f}(z,\tau) - \frac{1}{2}\Lambda z(z\xi(\tau) - 2) \\
S(z,\tau) &= z^2\mathrm{Sf}(z,\tau) + \frac{9\tau^2\xi(\tau) - 6\Lambda^2\tau^2 z + \frac{18\tau^2}{z} + 6\tau - 2z}{18\tau^{5/3}} \\
\dot{B}(z,\tau) &= z^3\dot{B}f(z,\tau) - \frac{2\left(\tau^2 - \tau z + z^2\right) + \tau z^2\xi(\tau)}{6\tau^3} \\
\dot{\phi}(z,\tau) &= z^2\dot{\phi}f(z,\tau) - \frac{\Lambda}{2} \\
A(z,\tau) &= z^2\mathrm{Af}(z,\tau) - \frac{2\Lambda^2}{3} - \xi'(\tau) + \frac{(z\xi(\tau) + 2)^2}{4z^2}
\end{aligned}
\tag{5.11}
$$

5.3 Gauge fixing and apparent horizon

One of the main problems we are facing now is that our numerical grid in the z direction cannot span the whole bulk. That would usually be a problem, since we would be missing some of the dynamics and our simulation would start accumulating numerical errors coming from the part we are not simulating. But there is a black hole inside the bulk cloaked by an event horizon, so we do not need to simulate anything inside this horizon since it will be causally disconnected from the boundary. Thus we only need to make sure our grid encapsulates the event horizon at all times.

We still have not fixed the gauge freedom $r \to r + \xi$ which shifts the whole system, so we can use it to move the horizon at will and make sure it is placed inside our grid. But the event horizon is a global concept and cannot be found until we have computed the full evolution and the system has reached equilibrium. Therefore we will compute the apparent horizon, which is local and can be computed numerically at every timestep. It is defined as the outermost trapped surface, that is, the outermost region in which geodesics pointing outward do not expand. This horizon is always inside the event horizon until the system reaches equilibrium, when both horizons will be the same. For our metric the apparent horizon is located at the value of z for which $\dot{S}(z,t) = 0$.

We will treat $\xi(t)$ as a dynamical variable and evolve it by requiring that the apparent horizon lies at a fixed radial coordinate $z = z_h$. At the beginning of the simulation we will compute the current value of the horizon z_H^* by finding the zero of the function

$\dot{S}(z,t)$. Then we can perform a gauge transformation with $\xi = 1/z_H^* - 1/z_H$, which will move the apparent horizon from z_H^* to our desired value z_H.

Next we want our horizon to stay fixed, so we should impose $\partial_t \dot{S}(z,t) = 0$, but there is no mechanism to bring it back to the desired value in case numerical instabilities move it away. So we will use the following equation taken from [1]:

$$\Big(\partial_t \dot{S}(z,t) + \kappa \dot{S}(z,t)\Big)\Big|_{z=z_h} = 0 \tag{5.12}$$

Where κ parameterizes the "strength" with which we pull the horizon back to its desired place. With the expression for $\partial_t \dot{S}$ taken from (5.5), this can be expressed as a differential equation for $\partial_t \xi(t)$, and thus we will be able to extract the time evolution of the gauge parameter $\xi(t)$ from requiring the horizon to always lie at $z = z_H$.

5.4 Evolution scheme

Now that we have properly defined the evolution equations and the finite variables we can define the evolution algorithm we will use:

1. Start with the profiles for $\phi(z,t_i)$ and $B(z,t_i)$ at a certain time step t_i and the values of $a4(t_i)$ and $\xi(t_i)$. From there we extract the profiles for the finite functions $\phi f(z,t_i)$ and $Bf(z,t_i)$.

2. Solve the Einstein equations (5.5) one by one to find the finite functions Sf, $\dot{S}f$, $\dot{B}f$, $\dot{\phi}f$ and finally Af. Use the boundary conditions from (5.8).

3. Compute the value of $\partial_t \dot{S}$ from numerical derivatives using previous timesteps, and compare this to the value from the last equation in (5.5). As explained before, store this to compute the numerical error.

4. From the profiles obtained for $\dot{\phi}(z,t_i)$ and $\dot{B}(z,t_i)$ get the profiles for $\partial_t \phi(z,t_i)$ and $\partial_t B(z,t_i)$ using (5.3). Compute the values for $\partial_t \xi(t)$ and $\partial_t a4(t)$ from (5.9) and (5.12).

5. From these time derivatives advance the profiles and values to the next timestep using the Adam-Bashforth method or similar. With the profiles for $\phi(z, t_{i+1})$, $B(z, t_{i+1})$, $a4(t_{i+1})$, $\xi(t_{i+1})$, go back to 1 and perform the next timestep.

So by giving initial conditions for $a_4(t_i)$, $B(t_i, z)$ and $\phi(t_i, z)$ and choosing an initial $\xi(t_i)$ such that the horizon lies at z_H as explained in the previous section, we can repeat these steps to get the evolution of all the observables and metric coefficients. To perform the discretization of our equations we will use a uniform time grid, and a Chebyshev grid for the radial coordinate z. This consists of $N+1$ points placed on:

$$X_i = \cos\left(\frac{\pi i}{N}\right) \quad i = (0, 1, ..., N), \tag{5.13}$$

which we can transform to our desired grid starting at $z = 0$ and ending at $z = z_f$ using:

$$Z_i = \frac{X_i + 1}{2} z_f \tag{5.14}$$

And from it we have computed the corresponding differentiation matrix to obtain the derivatives of the functions. On the other hand, since time derivatives are computed from a uniform grid we can use the well known Adams-Bashforth multistep methods.

5.5 Expectation values

Next we can compute the expectation values for the energy tensor components using the expressions obtained from holographic renormalization (2.12). By plugging in the near boundary expressions (5.6) into the expansions for $g_{\mu\nu}$ and ϕ we obtain:

$$\begin{aligned}
\tilde{\epsilon} &= \frac{L^3}{2\kappa_5^2}\left[-\frac{3a_4(t)}{4} - \lambda_4 \Lambda^4 + \frac{7\Lambda^4}{36} + \frac{1}{4}\Lambda^2\xi(t)^2 - \Lambda\phi_2(t)\right] \\
\tilde{P}_L &= \frac{L^3}{2\kappa_5^2}\left[-\frac{a_4(t)}{4} - 2b_4(t) + \lambda_4\Lambda^4 - \frac{5\Lambda^4}{108} - \frac{1}{12}\Lambda^2\xi(t)^2 + \frac{1}{3}\Lambda\phi_2(t)\right] \\
\tilde{P}_T &= \frac{L^3}{2\kappa_5^2}\left[-\frac{a_4(t)}{4} + b_4(t) + \lambda_4\Lambda^4 - \frac{5\Lambda^4}{108} - \frac{1}{12}\Lambda^2\xi(t)^2 + \frac{1}{3}\Lambda\phi_2(t)\right]
\end{aligned} \tag{5.15}$$

We give them a tilde to distinguish them from the hydrodynamic variables in (4.4). Also, using black hole thermodynamics and following a similar approach to the one done for the static solutions metric we can find expressions for entropy and temperature.

For the entropy we can compute again the determinant of the metric of the boundary

of the black hole, $\sqrt{Det(\gamma_{ij})} = S^3(z,t)$, which means that the entropy density is:

$$s = \frac{L^3}{2\kappa_5^2}\frac{4\pi S^3(z_H,t)}{L^3} \tag{5.16}$$

To compute the temperature we must do a similar procedure as before. By performing the change $dt \to dv + \frac{1}{A}dr$ we get rid of the cross term $2drdt$, and the metric becomes:

$$ds^2 = \frac{1}{A(r,v)}dr^2 - A(r,v)dv^2 + S(r,v)^2 e^{-2B(r,v)}dx_L^2 + S(r,v)^2 e^{B(r,v)}d\mathbf{x}_T^2 \tag{5.17}$$

Again we only focus on the dv^2 and dr^2 terms. Since the temperature is defined at the horizon we can make an expansion around r_H, where $A(r_H,(r,v)) = A_1(r-r_H,v)+\mathcal{O}(r-r_H)^2$. Defining a new coordinate $\rho^2 = r - r_H$ we get:

$$ds^2 = \frac{4}{A_1}d\rho^2 - A_1\rho^2 dv^2 \tag{5.18}$$

Now we can go to imaginary time τ and the metric becomes:

$$ds^2 = \frac{4}{A_1}d\rho^2 + A_1\rho^2 d\tau^2 \tag{5.19}$$

We want to avoid conical singularities, so we will change the coordinates to $d\rho \to \frac{\sqrt{A_1}}{2}d\tilde{\rho}$:

$$ds^2 = d\tilde{\rho}^2 + \frac{A_1^2}{4}\tilde{\rho}^2 d\phi^2 \tag{5.20}$$

This means, that to avoid conical singularities we find:

$$T = \frac{A_1}{4\pi} = \frac{\partial_r A(r,t)|_{r_H}}{4\pi} \tag{5.21}$$

Or in the coordinate z:

$$T = -\frac{z^2\partial_z A(z,t)|_{z_H}}{4\pi} \tag{5.22}$$

5.6 Numerical Checks

We want to make sure our code works well, so we will perform some simulations and see if the observables evolve as expected. We will start with the computation of the apparent horizon and the null geodesics.

In this metric outgoing radial null geodesics satisfy the following equation:

$$\frac{dr}{dt} = \frac{A(r,t)}{2} \tag{5.23}$$

$$\frac{dz}{dt} = -z^2\frac{A(z,t)}{2} \tag{5.24}$$

So now we can study the geodesics to see if they make sense. For example, we expect that close to the boundary the geodesics will behave as straight lines, since from the behaviour of $A(z,t)$ close to the boundary we get $\frac{dz}{dt} \approx -1/2$.

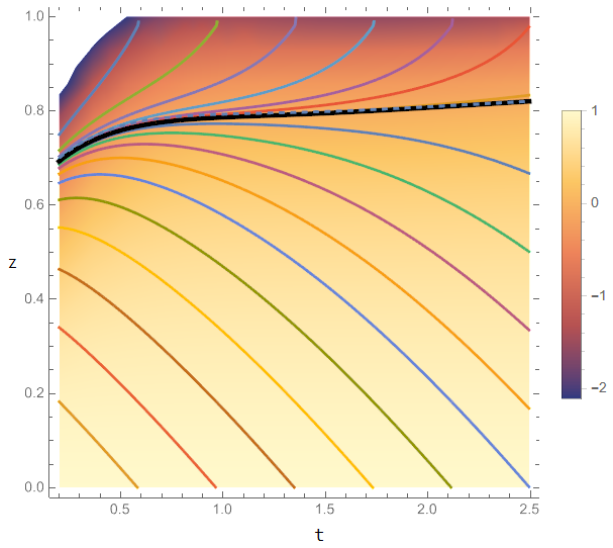

Figure 9: Congruence of outgoing radial null geodesics. The dashed line is the apparent horizon, and the thick black line is the event horizon. The background plot corresponds to $A(z,t)$.

As we expected in figure 9 the geodesics close to the boundary behave as straight lines with a slope of $-\frac{1}{2}$. Also, we can see that some geodesics plunge into the bulk while some escape, and they are separated by a geodesic that does neither, the event horizon colored in black. As we mentioned earlier the event horizon cannot be found locally until the metric has reached equilibrium, since future behaviour of the metric will dictate whether geodesics escape or not.

Next we want to make sure that the simulations are running smoothly and the numerical error is not too large, so we will study how the number of points in our grid affects the

accumulated error in our simulation. To do that we will first study how well energy-momentum conservation is satisfied and how the constraint behaves.

With energy-momentum conservation, for the homogeneous setting is as simple as energy density being constant, but for the boost invariant case it needs to satisfy

$$-\tau \frac{d}{d\tau} T_{\tau\tau} - T_{\tau\tau} + \frac{1}{\tau^2} T_{yy} = 0 \tag{5.25}$$

Or expressing it in terms of energy density and pressures,

$$\tau \frac{d\epsilon}{d\tau} + \epsilon + P_L = 0 \tag{5.26}$$

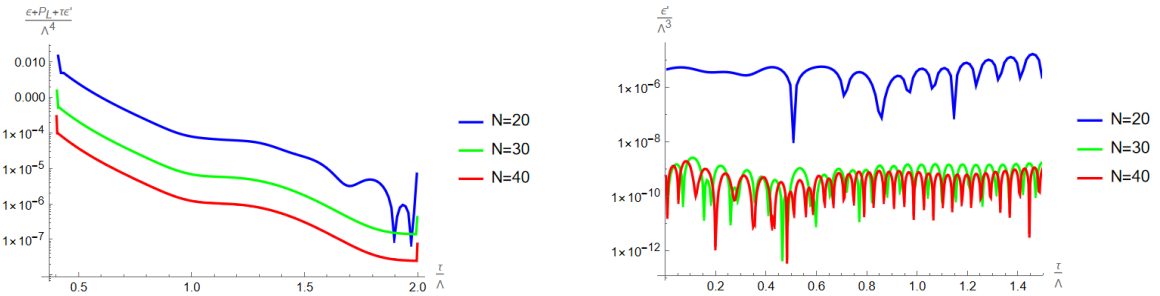

(a) **(b)**

Figure 10: Energy momentum conservation as a function of time for different values of the number of grid points N in the boost invariant setting (a) and the homogeneous setting (b).

As we increase the number of points in our grid the error associated to energy momentum decreases, and also the error change when going from 30 to 40 points is much smaller than the one going from 20 to 30.

We will also check if our dynamical simulations match the results of the static solutions. If we run different simulations on the homogeneous case we expect the system to relax towards the values found in static solutions and as seen in Figure 11 we can see they do.

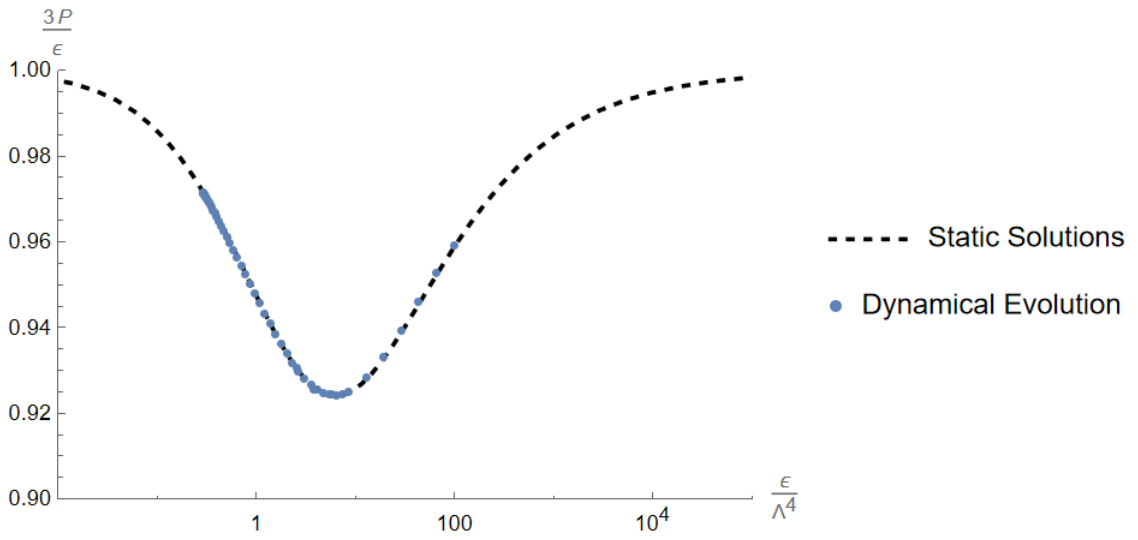

Figure 11: Results obtained from static solutions for $3P(\epsilon)/\epsilon$ for $\lambda_4 = 1/4$ compared to different dynamical evolutions with different initial energies. They both match.

5.7 Quasi-normal Modes

Another interesting test we can run is studying what happens to the system when we bring it away from equilibrium. To do it we will introduce perturbations to the black brane solutions we have found before in the homogeneous setting and study how they relax to their equilibrium state. This will tell us whether our system is stable with respect to perturbations, and will also help us to compare tabulated results and check if we are getting the correct results.

The relaxation back to equilibrium will be dictated by an infinite set of damped oscillatory modes called quasi-normal modes. We will study the different channels for relaxation and how their frequencies depend on temperature. We are restricting ourselves to the homogeneous setting because we only want to study the $k = 0$ modes. Also, in the boost invariant setting frequencies would change with temperature and thus with time, making it not a suitable setup.

If we denote the metric inside the bulk in Eddington Finkelstein coordinates as G, a general perturbation from equilibrium will be:

$$G_{MN} \to G_{MN} + h_{MN}, \quad \phi \to \phi + \varphi. \tag{5.27}$$

There will be two distinct channels for this excitations to relax, the anisotropy and the bulk channels. The former will control variations in the anisotropy of the metric, given in our coordinates by $B(z,t)$. These oscillations only affect the difference between longitudinal and transversal pressures, without changing the expectation value of the scalar field, the trace of the stress energy tensor or the average pressure.

The latter will be a non-conformal mode that will change the trace of the stress-tensor, the scalar field and the mean pressure, all without changing the anisotropy of the system. These two channels will be completely independent.

5.7.1 Numerical procedure

To find these modes we will start a simulation slightly out of equilibrium, and evolve the system letting it relax towards it. For the anisotropy channel we will study the behaviour of $b_4(t)$, since it does not contribute to the trace of $T_{\mu\nu}$ and controls the anisotropy of the system. For the bulk channel we will study the behaviour of $\phi_2(t)$ because it does contribute to the trace but has nothing to do with anisotropy or difference between pressures.

The behaviour of these variables should be given by an infinite tower of dampened oscillatory modes, but for this project we will only focus on the leading quasinormal mode which is the one our numerics are sensitive to. To find it we will try to fit them with the following function:

$$f(t) = C_0 + A\cos(\omega_r t + \psi)e^{-\omega_i t}, \tag{5.28}$$

where C_0 is an offset that will only be present for the bulk channel, since in equilibrium there is no anisotropy and thus the value will oscillate around zero. At early times the perturbation might be too large and thus the system would not be in the linear regime, rendering our approximation incorrect. So we will perform a series of fits, each starting at a later time. Then we will obtain the parameters of the fit, and compute the limiting value as we go to later times.

If we wanted to find the higher order quasi-normal modes we would subtract the expression for the first quasi-normal mode from the data, and repeat the procedure to find the new frequencies. We could find all the modes independently because the amplitude of each mode is a few orders of magnitude smaller than the last one.

To get an idea of how these modes look, here are the profiles for $b_4(t)$ and $\phi_2(t)$ for $\lambda_4 = 1/4$, $\lambda_6 = 1/10$: But it is hard to see if they are well described by our function

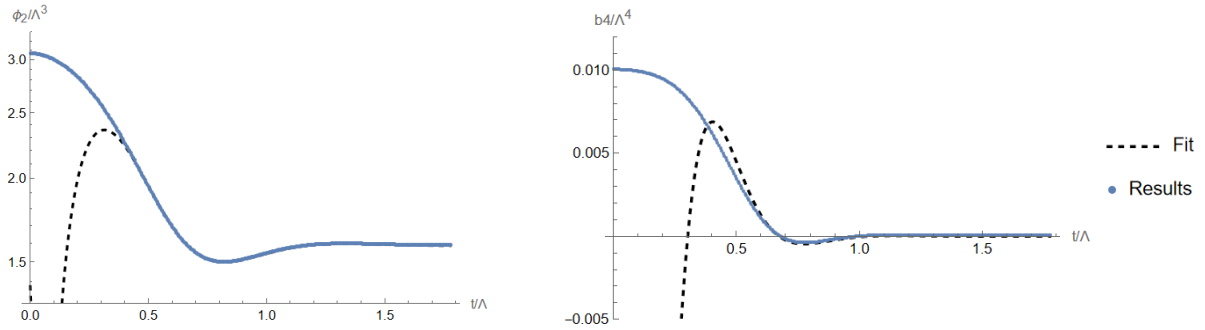

(a) **(b)**

Figure 12: Evolution profiles for (a) $\phi_2(t)$ and (b) $b_4(t)$ with their respective numerical fits. As expected they both oscillate around an equilibrium value with a dampened motion. b_4 will always oscillate around 0.

(5.28), so let us plot the function together with the fit in a logarithmic plot (Fig 13). As

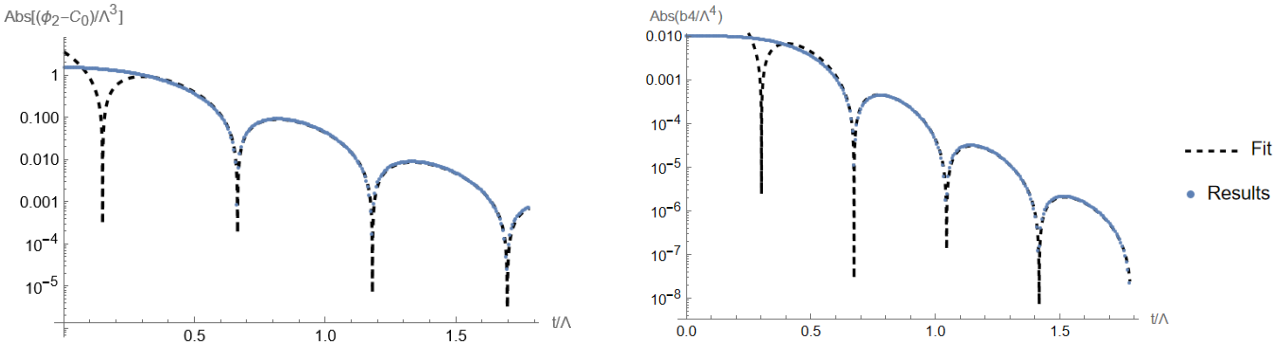

(a) **(b)**

Figure 13: Evolution profiles for (a) $\phi_2(t)$ and (b) $b_4(t)$ with their respective numerical fits in a log plot.

expected for earlier times the system is too far out of equilibrium, and so the system is not in the linear regime and the relaxation is not according to these modes. But for later times the fit reproduces the behaviour properly.

Then we can compute the frequencies of these modes as a function of temperature, which in the case of the anisotropy channel yields:

It follows that these frequencies grow approximately linearly with temperature. Although the plot for the bulk channel frequencies seem to behave in a different way at low temperatures we believe that it is due it still not being close to the CFT, where the assumption

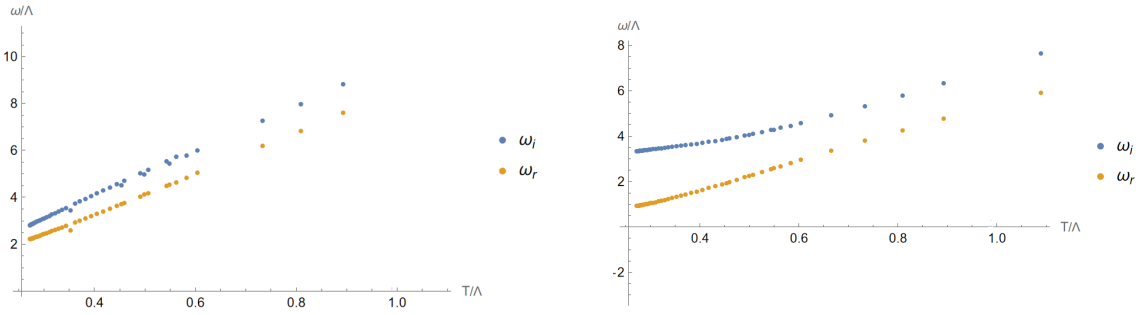

(a) **(b)**

Figure 14: Real and imaginary frequencies for the anisotropy (a) and bulk (b) channels as a function of temperature for $\lambda_4 = 1/4$.

$\omega \propto T$ should apply. which means that the cooler the system is the longer it will take for it to relax towards equilibrium, which might be worrying, because if for some reason we are driven out of equilibrium at late times then the expansion might be driving it away too fast from equilibrium for the system to go back towards it. For this to happen the rate of expansion $1/\tau$ would have to be faster than the quasinormal frequencies. Since at late times in the boost invariant we will be at the IR limit and thus in a CFT, the temperature goes as $T \sim \epsilon^{1/4} \sim \tau^{-1/3}$. That means that the ratio of frequencies to expansion goes as:

$$\frac{\omega}{1/\tau} \approx \frac{T}{\tau^{-1}} \approx \frac{\tau^{-1/3}}{\tau^{-1}} \approx \tau^{2/3} \tag{5.29}$$

So the relaxation rate will grow faster than the expansion rate, and we will not be thrown away from equilibrium.

5.8 Results

Now that we have a code to perform dynamical evolutions and we are confident it works, we can start studying the behaviour of the plasma. First we will study if hydrodynamics is a good approximation to our system for late times. To do this we will run a dynamical evolution and obtain the profile for $\epsilon(\tau)$. Then, using our static solutions and this profile we will be able to find the values for $\eta(\tau)$ and $\zeta(\tau)$ and $P(\tau)$, which will allow us to compute $P_L(\tau)$ and $P_T(\tau)$ from (4.11) and compare them to the measured results. If we do so we find:

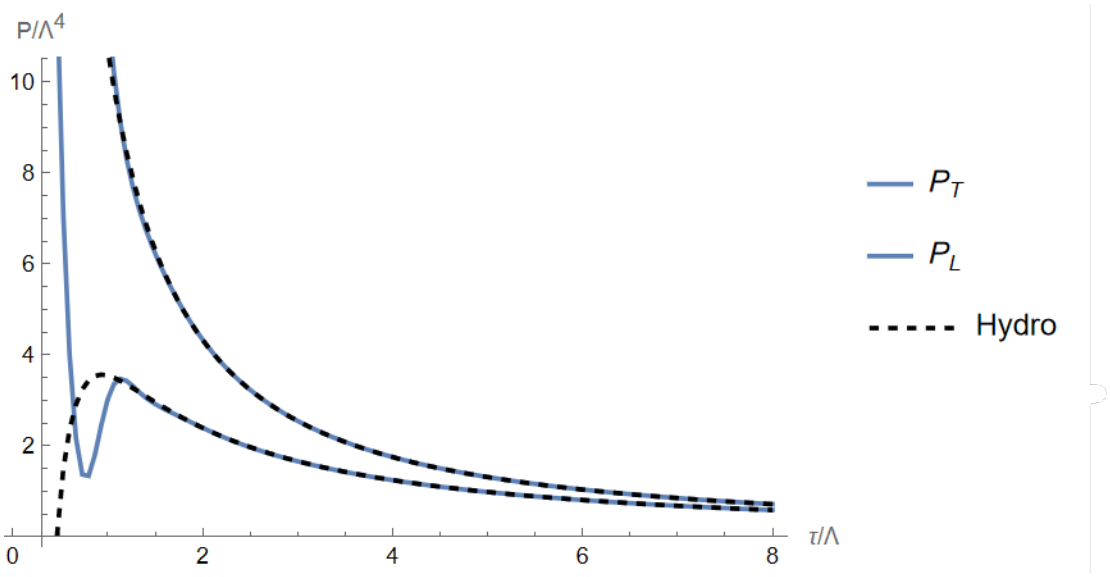

Figure 15: Transverse and longitudinal pressures as a function of time with their respective first order hydrodynamic fits for $\lambda_4 = 1/4$.

And if we study how the relative error associated with the fit evolves over time, we can clearly see that as the system relaxes towards equilibrium the hydrodynamic approximation gets better.

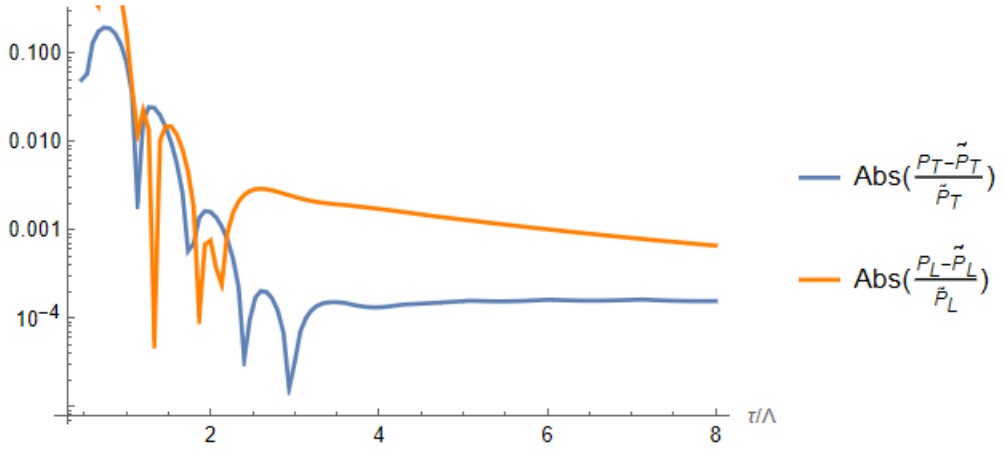

Figure 16: Relative error of the hydrodynamic pressures as a function of time

Now let us study the generality of these results, since we want to avoid having results that depend on finely tuned initial conditions. We have run 8 simulations with different initial conditions but the same initial energy, and studied how the system hydrodynamizes. In figure 17 can again see that for all different initial conditions the system tends towards the same band and a similar behaviour that is well described by hydrodynamics.

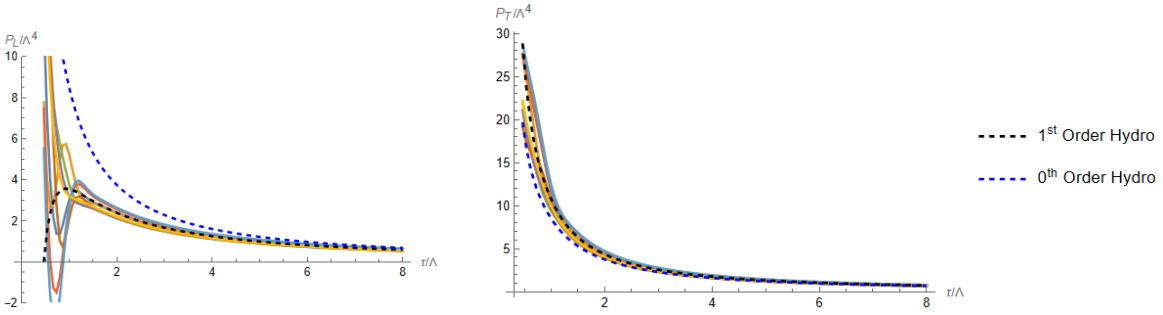

(a) **(b)**

Figure 17: Numerical simulations for the longitudinal and transverse pressures for one simulation of the plasma expansion, together with a zero and first order hydrodynamic approximations.

Next we will study what happens to the system when undergoing the phase transition we studied at the beginning of this thesis. Usually we would expect that as soon as the system enters the spinodal branch it will become unstable and the system will spontaneously separate into two phases. Then as it cools down even more the proportion of phases in coexistence will change until we only have the phase with less energy and the system leaves the spinodal branch.

But in our microscopic simulation we will not find this phase separation, since our system does not have spatial dependencies and it cannot present inhomogeneities. This will mean that no phase separation can occur and thus it will be able to run along the spinodal branch unimpeded. If we run the simulation for different initial conditions we see that this is true, and the system performs the characteristic "s" shape. As can be seen the dynamic curve followed by the simulations is separated from the one obtained through static solutions, and that separation is given by the hydrodynamic corrections. By starting the simulation at different times we can make these corrections larger or smaller.

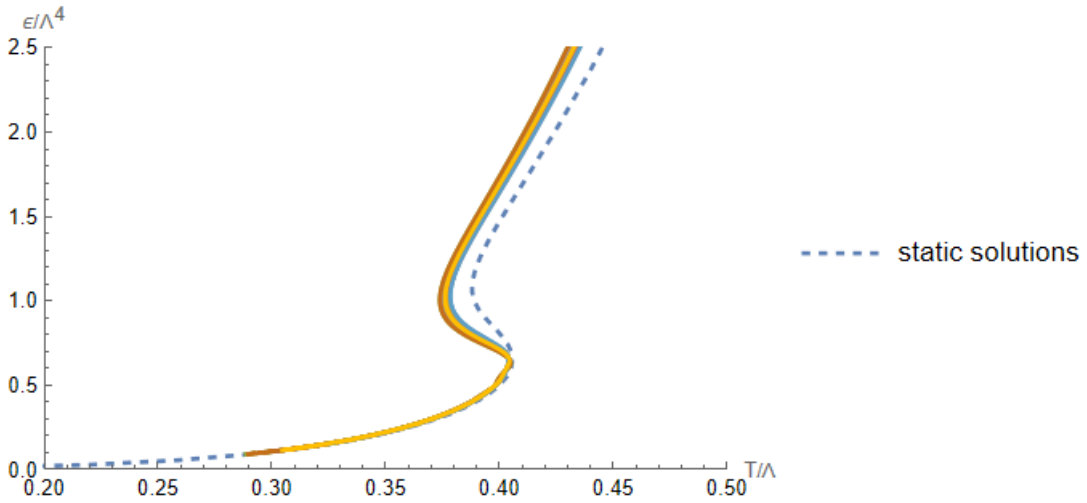

Figure 18: Numerical simulations for $\lambda_4 = -1/4$ with 8 different initial conditions but the same initial energy, compared to the results obtained from static solutions.

6 Discussion

In this project we built an holographic model to describe the properties of QCD. We have computed its equilibrium as well as the dynamic solutions, and studied its thermodynamic structure revealing a second order phase transition for some values of the parameters characterizing the scalar field potential potential.

We then studied the dynamical evolution of the system in the boost invariant setting, which models the expansion of quark gluon plasma resulting from a high energy heavy ion collision. We compared it to the predicted values for longitudinal and transverse pressure and saw that it was well described by it at some relatively early time.

While this model is able to study the properties of the phase transition by computing static solutions it is not able to properly describe how the system undergoes this transition as it is cooling down. Since we do not allow for inhomogeneities the system is not able to undergo the phase transition at the critical temperature and will explore the unstable spinodal branch.

This leaves many questions open that would interesting to study. The first one and the simplest is to perform the evolutions in the phase transition regime as in figure 18 but starting at different initial times. If the simulation starts at a later time then the hydrodynamic corrections are smaller and thus the system would be closer to the static curve and it should follow the "s" shape more closely. But if the simulation starts at earlier times then viscous corrections would be more significant and the system would evolve far from the static curve. It would be interesting to see if the system would undergo this phase transition or since it is so far away from it it would just go towards the stable phase in a smooth manner.

Also it would be interesting to relax our ansatz for the EF coordinates (5.1) and allow for inhomogeneities in the plasma. This would allow for phase separation to happen and we might get the expected behaviour of a second order phase transition.

Acknowledgements

I would like to thank my first supervisor, Wilke van der Schee, for his guidance throughout the whole project. I also want to thank Javier Subils, my daily supervisor, for his patience and support while debugging our code and running it in his far more powerful computer. He made himself available to answer my questions and solve my problems since the beginning, and I am very grateful.

I want to thank Marc Aragonès, with whom I have been working together during part of this thesis, and we have helped each other to understand some concepts or bugs in the code which otherwise would have taken me longer to understand.

Finally I would also like to thank David Mateos for giving us some helpful insights into this project, as well as my partner Fiona Román and my whole family for giving me emotional support throughout.

Bibliography

[1] Maximilian Attems et al. "Paths to equilibrium in non-conformal collisions". In: *Journal of High Energy Physics* 2017.6 (June 2017). ISSN: 1029-8479. DOI: 10.1007/jhep06(2017)154. URL: http://dx.doi.org/10.1007/JHEP06(2017)154.

[2] Maximilian Attems et al. "Thermodynamics, transport and relaxation in non-conformal theories". In: *Journal of High Energy Physics* 2016.10 (Oct. 2016). ISSN: 1029-8479. DOI: 10.1007/jhep10(2016)155. URL: http://dx.doi.org/10.1007/JHEP10(2016)155.

[3] Rudolf Baier et al. "Relativistic viscous hydrodynamics, conformal invariance, and holography". In: *Journal of High Energy Physics* 2008.04 (Apr. 2008), pp. 100–100. ISSN: 1029-8479. DOI: 10.1088/1126-6708/2008/04/100. URL: http://dx.doi.org/10.1088/1126-6708/2008/04/100.

[4] Jacob D. Bekenstein. "Black Holes and Entropy". In: *Phys. Rev. D* 7 (8 Apr. 1973), pp. 2333–2346. DOI: 10.1103/PhysRevD.7.2333. URL: https://link.aps.org/doi/10.1103/PhysRevD.7.2333.

[5] Massimo Bianchi, Daniel Z. Freedman, and Kostas Skenderis. "Holographic renormalization". In: *Nuclear Physics B* 631.1–2 (June 2002), pp. 159–194. ISSN: 0550-3213. DOI: 10.1016/s0550-3213(02)00179-7. URL: http://dx.doi.org/10.1016/S0550-3213(02)00179-7.

[6] Massimo Bianchi, Daniel Z. Freedman, and Kostas Skenderis. "How to go with an RG flow". In: *JHEP* 08 (2001), p. 041. DOI: 10.1088/1126-6708/2001/08/041. arXiv: hep-th/0105276.

[7] J. D. Bjorken. "Highly relativistic nucleus-nucleus collisions: The central rapidity region". In: *Phys. Rev. D* 27 (1 Jan. 1983), pp. 140–151. DOI: 10.1103/PhysRevD.27.140. URL: https://link.aps.org/doi/10.1103/PhysRevD.27.140.

[8] Jorge Casalderrey-Solana et al. *Gauge/String Duality, Hot QCD and Heavy Ion Collisions*. 2012. arXiv: 1101.0618 [id='hep-th'].

[9] Paul M. Chesler and Laurence G. Yaffe. "Numerical solution of gravitational dynamics in asymptotically anti-de Sitter spacetimes". In: *Journal of High Energy Physics* 2014.7 (July 2014). ISSN: 1029-8479. DOI: 10.1007/jhep07(2014)086. URL: http://dx.doi.org/10.1007/JHEP07(2014)086.

[10] Christopher Eling and Yaron Oz. "A novel formula for bulk viscosity from the null horizon focusing equation". In: *Journal of High Energy Physics* 2011.6 (June 2011). ISSN: 1029-8479. DOI: 10.1007/jhep06(2011)007. URL: http://dx.doi.org/10.1007/JHEP06(2011)007.

[11] Antón F. Faedo et al. *Light holographic dilatons near critical points*. 2024. arXiv: 2406.04974 [hep-th]. URL: https://arxiv.org/abs/2406.04974.

[12] S. W. Hawking. "Black holes and thermodynamics". In: *Phys. Rev. D* 13 (2 Jan. 1976), pp. 191–197. DOI: 10.1103/PhysRevD.13.191. URL: https://link.aps.org/doi/10.1103/PhysRevD.13.191.

[13] Romuald A. Janik. "Viscous Plasma Evolution from Gravity Using Anti–de Sitter/Conformal-Field-Theory Correspondence". In: *Physical Review Letters* 98.2 (Jan. 2007). ISSN: 1079-7114. DOI: 10.1103/physrevlett.98.022302. URL: http://dx.doi.org/10.1103/PhysRevLett.98.022302.

[14] Romuald A. Janik and Robi Peschanski. "Asymptotic perfect fluid dynamics as a consequence of AdS/CFT correspondence". In: *Physical Review D* 73.4 (Feb. 2006). ISSN: 1550-2368. DOI: 10.1103/physrevd.73.045013. URL: http://dx.doi.org/10.1103/PhysRevD.73.045013.

[15] Juan Maldacena. "The Large N Limit of Superconformal Field Theories and Supergravity". In: *International Journal of Theoretical Physics* 38.4 (1999), pp. 1113–1133. ISSN: 0020-7748. DOI: 10.1023/a:1026654312961. URL: http://dx.doi.org/10.1023/A:1026654312961.

[16] S. Ryu et al. "Importance of the Bulk Viscosity of QCD in Ultrarelativistic Heavy-Ion Collisions". In: *Phys. Rev. Lett.* 115 (13 Sept. 2015), p. 132301. DOI: 10.1103/PhysRevLett.115.132301. URL: https://link.aps.org/doi/10.1103/PhysRevLett.115.132301.

[17] Peter Steinberg. "Landau Hydrodynamics and RHIC Phenomena". In: *Acta Physica Hungarica A) Heavy Ion Physics* 24.1–4 (Oct. 2005), pp. 51–57. ISSN: 1588-2675. DOI: 10.1556/aph.24.2005.1-4.8. URL: http://dx.doi.org/10.1556/APH.24.2005.1-4.8.